Correction to "Three-dimensional nonlinear evolution of equatorial ionospheric bubbles with gravity wave seeding and tidal wind effects"

Sharon L. Vadas and M. J. Keskinen

Received 1 October 2009; published 2 February 2010.

Citation: Vadas, S. L., and M. J. Keskinen (2010), Correction to "Three-dimensional nonlinear evolution of equatorial ionospheric bubbles with gravity wave seeding and tidal wind effects," *Geophys. Res. Lett.*, *37*, L03101, doi:10.1029/2009GL041216.

[1] In the paper "Three-dimensional nonlinear evolution of equatorial ionospheric bubbles with gravity wave seeding and tidal wind effects" by M. J. Keskinen and Sharon L. Vadas (*Geophysical Research Letters*, *36*, L12102, doi:10.1029/2009GL037892), *Keskinen and Vadas* [2009, hereafter KV09] presented the three-dimensional nonlinear evolution of equatorial ionospheric bubbles using a realistic lower atmospheric gravity wave (GW) source. There are a number of misrepresentations and errors by KV09 in regards to the presentation and discussion of the GW source function that was used in the plasma model. The figures and discussion of KV09 refer to a different GW specification, despite the fact that the correct GW specification was used in the plasma model, results of which are presented in Figure 4 of KV09. As a result, the model data shown in Figures 1, 2, and 3 of KV09 were not used to seed the 3D plasma model described by KV09. Correct Figures 1–3 are supplied in this erratum. Additionally, part of paragraph 8 and all of paragraphs 9, 10, and 11 of KV09 should be disregarded and replaced with the text below.

[2] The dispersion relation discussed in the latter portion of paragraph 8 in KV09 was not the GW dispersion relation, but was rather the full complex dispersion relation derived from the compressible fluid equations by *Vadas and Fritts* [2005, hereafter VF2005]. Due to formula errors in KV09, readers interested in the compressible dispersion relation should refer directly to VF2005. The last half of paragraph 8 in VF09 should be replaced by the following: For anelastic GWs with horizontal phase speeds much less than the speed of sound, the GW dispersion relation is given by equation (26) from VF2005 or by equation (47) from *Vadas and Fritts* [2009, hereafter VF2009].

[3] *Vadas and Liu* [2009, Figure 1] shows a GOES-12 satellite image on 01 October, 2005, at 21:22 UT, in Brazil. For the KV09 study, we simulated the GWs excited by the energetic convective cluster at 59.0°W and 13.5°S. This cluster contained several tightly-clumped convective plumes, each having an approximate full-width horizontal diameter of 20 km and updraft velocities of ∼40 m/s. We defined a convective cluster to be composed of 3 convective plumes in an equilateral triangle configuration, with a separation of 50 km between the plume centers (VF2009). Figure 1 shows the GW spectrum excited by this cluster. Figure 1 replaces KV09's Figure 1. This cluster excites GWs with horizontal wavelengths of $\lambda_H > 100$ km and vertical wavelengths of $\lambda_z > 50$ km, which are capable of penetrating well into the thermosphere prior to dissipating [*Vadas*, 2007; *Fritts and Vadas*, 2008].

[4] The ray trace model we used was described by VF2009. The hyperbolic tanh zonal wind and temperature models shown in Figure 2 of KV09 were not used in either the ray trace or plasma models. Instead, the wind and temperature models we used were determined mainly from the Thermosphere-Ionosphere-Mesosphere-Electrodynamics General Circulation Model. *Vadas et al.* [2009] describe the background wind and temperature models used. Because they include semidiurnal and diurnal tides, both zonal and meridional background wind components were present.

[5] The GWs whose spectrum is plotted in Figure 1 were located at 59.0°W and 13.5°S at an altitude of $z = 13.6$ km at 21:22 UT. Those GWs were then ray traced into the middle and upper atmosphere through the spatially and temporally-varying background winds and temperatures. We then reconstructed the GW wind, temperature, and density perturbations as a function of (x, y, z, t) using the method described by VF2009. We extracted the vertical profiles (cuts) of this solution at 10 different locations and times. These profiles were inputted into the 3D plasma model

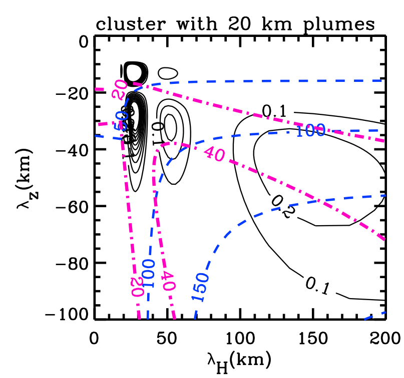

Figure 1. Vertical flux of zonal momentum as a function of horizontal and vertical wavelengths for the GWs excited by the convective cluster in increments of 10% of an arbitrary value (solid lines). We do not show the largest values here in order to emphasize the large-wavelength portion of the spectrum (which have smaller amplitudes). The form of the spectrum is given by equation (35) from VF2009. Pink dash-dot lines indicate the vertical group velocity $c_{gz} = \partial\omega_{Ir}/\partial m$ in intervals of 20 m/s. Blue dash lines indicate the intrinsic horizontal phase speed $c_{IH} = \omega_{Ir}/k_H$ in intervals of 50 m/s. Here, ω_{Ir} is the intrinsic frequency, and k_H and m are the horizontal and vertical wavenumbers, respectively.

0094-8276/10/2009GL041216$05.00

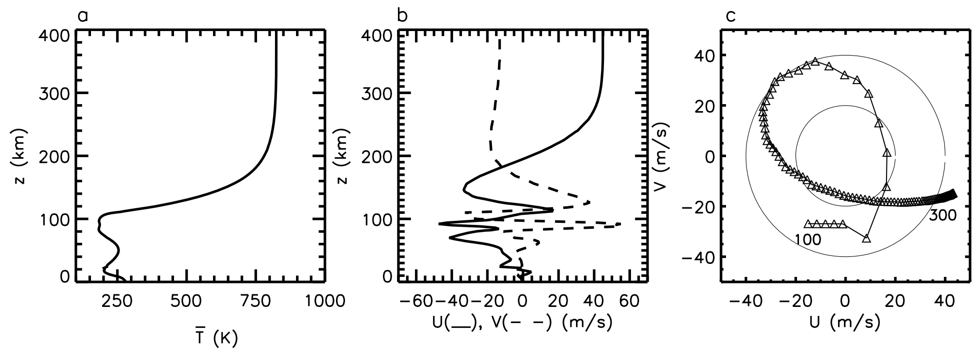

Figure 2. Background ("mean") profiles at 55.9°W, 11.0°S, and 22:32 UT on 01 October, 2005 in Brazil. (a) Temperature. (b) Zonal (solid) and meridional (dashed) background winds. (c) Hodograph of zonal and meridional background winds from z = 100 km (labeled "100") to z = 300 km (labeled "300") (triangles). Triangles are separated by 2 km vertically.

individually. Cut #2 was found to be optimum in producing plasma bubbles; this cut was used to produce KV09's Figure 4. Cut #2 was located at 55.9°W, 11.0°S, and 22:32 UT, which was ~440 km northeast of the cluster.

[6] Figure 2 shows the background (or "mean") temperature and horizontal wind profiles at the location and time of cut #2. Figure 2 replaces KV09's Figure 2. Here, $\overline{T}$ is temperature, and U and V are the zonal and meridional neutral wind components, respectively, in geographic coordinates. Figure 2c shows that the winds rotate counterclockwise with altitude at this southern hemisphere location (unlike the winds in Figure 2 of KV09).

[7] Figure 3 shows the GW parameters and amplitudes as a function of altitude for cut #2. Figure 3 replaces KV09's Figure 3. Here, the zonal, meridional, and vertical wavelengths are λ_x, λ_y and λ_z, respectively, the horizontal wavelength is $\lambda_H = [(\lambda_x)^{-2} + (\lambda_y)^{-2}]^{-1/2}$, the observed wave frequency is ω_r, the intrinsic frequency is $\omega_{Ir} = \omega_r - kU - lV$, $k = 2\pi/\lambda_x$, and $l = 2\pi/\lambda_y$. Here, overlines denote bin averages using the vertical flux of horizontal momentum (see equation (66) of VF2009). The irregular values of $\overline{\lambda_x}$, $\overline{\lambda_y}$, and $\overline{\lambda_z}$ in Figures 3a and 3b at $z \sim 240$ km are not significant because the GW amplitudes are quite small there, and occur because there are few waves which pass through these bins. Note that the GWs are mostly eastward-propagating because $|\lambda_x| < |\lambda_y|$. At $z \sim 200$–240 km, $\overline{\lambda_H} \sim 100$ km, $\overline{\lambda_z} \sim 70$ km, $\overline{\tau_r} \sim 10$–$12$ min, and $\overline{\tau_{Ir}} \sim 10$ min. Note that $\overline{\tau_{Ir}}$ is close to the buoyancy period of $\tau_b \sim 8$ min.

[8] The reconstructed GW zonal, meridional, and vertical velocities are u', v', and w', respectively, and are shown in Figures 3e and 3f. The reconstructed GW temperature and density perturbations are $T'/\overline{T}$ and $\rho'/\overline{\rho}$, respectively, and are

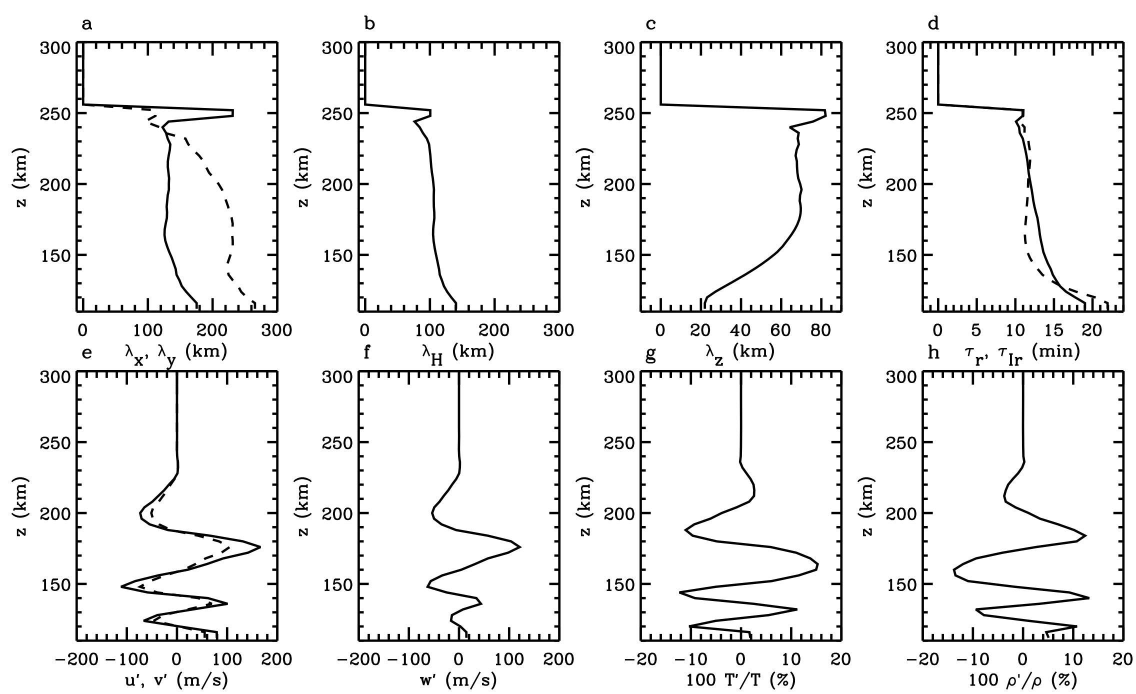

Figure 3. Average GW parameters and reconstructed GW solution along vertical cut #2. (a) $\overline{\lambda_x}$ (solid line) and $\overline{\lambda_y}$ (dashed line) in km. (b) $\overline{\lambda_H}$ in km. (c) $\overline{\lambda_z}$ in km. (d) $\overline{\tau_r}$ (solid line) and $\overline{\tau_{Ir}}$ (dashed line) in min. (e) u' (solid line) and v' (dashed line) in m/s. (f) w' in m/s. (g) 100 $T'/\overline{T}$. (h) 100 $\rho'/\overline{\rho}$.

shown in Figures 3g and 3h. We see that u', v', and w' are in phase, as expected for eastward, northward, and upward-propagating GWs. The GW amplitudes increase rapidly with altitude up to $z \sim 180$ km, and decrease with altitude for $z > 180$ km. These results are consistent with previous results [*Fritts and Vadas*, 2008]. The GW amplitudes are reasonably large for $z < 240$ km, with maxima of $u' \sim 160$ m/s, $v' \sim 100$ m/s, and $w' \sim 120$ m/s at $z \sim 180$ km. The temperature and density perturbations have similar amplitudes and are 180° out of phase, as expected [*Vadas and Liu*, 2009, equation (20)]. The maximum density and temperature perturbations are ~15%. These are consistent with previous estimates that $T'/T \sim 1\%$ corresponds to a horizontal velocity perturbation of $u'_H = \sqrt{(u')^2 + (v')^2} \sim$ 10 m/s [*Vadas et al.*, 2009, equation (17)]; scaling by a factor of 15, this implies that $T'/T \sim 15\%$ corresponds to $u'_H \sim$ 150 m/s, consistent with Figure 3e.

[9] **Acknowledgments.** SLV would like to thank M.J. Nicolls for his help with this manuscript. This work was supported by NASA contract NNH07AF50I.

References

Fritts, D. C., and S. L. Vadas (2008), Gravity wave penetration into the thermosphere: Sensitivity to solar cycle variations and mean winds, *Ann. Geophys.*, *26*, 3841–3861.

Keskinen, M. J., and S. L. Vadas (2009), Three-dimensional nonlinear evolution of equatorial ionospheric bubbles with gravity wave seeding and tidal wind effects, *Geophys. Res. Lett.*, *36*, L12102, doi:10.1029/2009GL037892.

Vadas, S. L. (2007), Horizontal and vertical propagation and dissipation of gravity waves in the thermosphere from lower atmospheric and thermospheric sources, *J. Geophys. Res.*, *112*, A06305, doi:10.1029/2006JA011845.

Vadas, S. L., and D. C. Fritts (2005), Thermospheric responses to gravity waves: Influences of increasing viscosity and thermal diffusivity, *J. Geophys. Res.*, *110*, D15103, doi:10.1029/2004JD005574.

Vadas, S. L., and D. C. Fritts (2009), Reconstruction of the gravity wave field from convective plumes via ray tracing, *Ann. Geophys.*, *27*, 147–177.

Vadas, S. L., and H. Liu (2009), Generation of large-scale gravity waves and neutral winds in the thermosphere from the dissipation of convectively generated gravity waves, *J. Geophys. Res.*, *114*, A10310, doi:10.1029/2009JA014108.

Vadas, S. L., M. J. Taylor, P.-D. Pautet, P. A. Stamus, D. C. Fritts, H.-L. Liu, F. T. Sao Sabbas, V. T. Rampinelli, P. Batista, and H. Takahashi (2009), Convection: The likely source of the medium-scale gravity waves observed in the OH airglow layer near Brasilia, Brazil, during the SpreadFEx campaign, *Ann. Geophys.*, *27*, 231–259.